Clinical trial of time-resolved scanning optical mammography at 4 wavelengths between 683 and 975 nm

Paola Taroni
Politecnico di Milano
INFM—Dipartimento di Fisica
    and
IFN-CNR
Piazza Leonardo da Vinci 32
I-20133 Milan
Italy
E-mail: paola.taroni@fisi.polimi.it

Gianmaria Danesini
Casa di Cura S.Pio X
Dipartimento di Radiologia
via Francesco Nava 31
I-20159 Milan
Italy

Alessandro Torricelli
Antonio Pifferi
Lorenzo Spinelli
Rinaldo Cubeddu
Politecnico di Milano
INFM—Dipartimento di Fisica
    and
IFN-CNR
Piazza Leonardo da Vinci 32
I-20133 Milan
Italy

Abstract. The first time-resolved optical mammograph operating beyond 900 nm (683, 785, 913, and 975 nm) is presently being used in a clinical trial to test the diagnostic potential of the technique in detecting and characterizing breast lesions. Between November 2001 and October 2002, 101 patients with malignant and benign lesions were analyzed retrospectively. Scattering plots, as derived from a homogeneous model, and late gated intensity images, to monitor spatial changes in the absorption properties, are routinely used. The intensity images available at four wavelengths provide sensitivity to the main tissue constituents (oxy- and deoxyhemoglobin, water, and lipids), in agreement with expected tissue composition and physiology, while the scattering plots mirror structural changes. Briefly, tumors are usually identified due to the strong blood absorption at short wavelengths, cysts to the low scattering, and fibroadenomas to low absorption at 913 nm and high at 975 nm, even though the optical features of fibroadenomas seem not to be uniquely defined. The effectiveness of the technique in localizing and discriminating different lesion types is analyzed as a function of various parameters (lesion size, compressed breast thickness, and breast parenchymal pattern). © *2004 Society of Photo-Optical Instrumentation Engineers.* [DOI: 10.1117/1.1695561]

Keywords: optical mammography; breast; photon migration; tumor.

Paper 44007 received Jul. 1, 2003; revised manuscript received Jan. 15, 2004; accepted for publication Jan. 16, 2004.

1 Introduction

Extensive clinical studies on conventional breast transillumination performed in the 1980s showed low sensitivity and specificity,[1–3] but later technical developments opened new possibilities to optical diagnostic methods. In recent years, both in the U.S. and Europe, optical mammography has being investigated as a possible means for the diagnosis of breast cancer. Several approaches, for both projection imaging and tomography, in some cases even exploiting exogenous contrast agents, have been considered and are presently being tested *in vivo*.[4–6] Up to now, systematic clinical studies have usually been carried out with instruments operating in projection geometry, in continuous wave (cw),[7] or in the frequency domain[8,9] at wavelengths between 670 and 860 nm, i.e., in the spectral range of maximum light transmission through breast tissue.

A multicentric clinical trial is now being performed, supported by the European project OPTIMAMM, to test the diagnostic potential of time domain techniques for optical mammography, and initial clinical results at 670 and 785 nm were published very recently by two partners.[10]

The near-infrared (NIR) range that is typically considered for *in vivo* applications of optical methods (650 to 800 nm) is primarily sensitive to the blood content in tissue. Actually,

most NIR instruments were developed for oximetry and related uses. Consequently, the attention was focused on assessing the concentration of the two forms of hemoglobin and the oxygen saturation in tissues. On the other hand, for what concerns breast cancer detection, the sensitivity and the specificity of optical techniques are expected to improve if they could be sensitive not only to the blood content, but also to other tissue constituents and physiological parameters. X-ray mammography is characterized by very high spatial resolution, and its diagnostic effectiveness resides in its capacity to detect even very fine morphological changes. In this respect, optical mammography cannot compete with conventional mammography.[11,12] However, the inherent potential of optical techniques is in their spectroscopic content that can provide physiological information.[13–15] This could be achieved by extending the spectral range of operation. Shorter wavelengths might be of interest, but the attenuation in tissues is usually prohibitive for clinical applications when short measurement times are a given requirement. Strong light attenuation also occurs at longer wavelengths. Moreover, no suitable commercial detectors were available for time-resolved measurements. Taking advantage of a recently developed custom photomultiplier tube (PMT), we have decided to extend the operation range of our instrument beyond 900 nm, in a region characterized by absorption peaks of two major constituents of

Address all correspondence to Paola Taroni, Politecnico di Milano, Dipartimento di Fisica, Piazza Leonardo da Vinci 32, 20133 Milan, Italy. Tel: +39-02-2399-6109; FAX: +39-02-2399-6126; E-mail: paola.taroni@fisi.polimi.it

breast tissue: lipids at 930 nm and water at 970 nm.[16,17] Our research group at Politecnico has developed and tested a time-resolved scanning instrument operating at 683, 785, 913, and 975 nm. Up to October 2002, its clinical trial within the European Union (EU) project has involved 101 patients with malignant and benign lesions. The present work reports about the results of this first part of the clinical trial.

2 Instrument Setup and Measurement Protocol

The instrument is designed to collect projection images of the breast compressed between plane Plexiglas plates, in the same geometry as used in conventional x-ray mammography, but with a milder degree of compression. Four pulsed-diode lasers (PDL Heads, PicoQuant, Germany) emitting at 683 and 785 nm [visible (VIS)], and at 913 and 975 nm (NIR), with average output power of ~1 to 4 mW, temporal width of ~180 to 400 ps (full-width at half maximum—FWHM), and repetition rate of 40 MHz, are used as light sources. A single driver (PDL-808 Sepia, PicoQuant, Germany) controls all four laser heads, and their output pulses are properly delayed by means of graded index optical fibers, and combined into a single coupler. A lens produces a 3-mm-diam collimated beam that illuminates the breast. A 5.6-mm-diam, 1-m-long fiber bundle collects the output light on the opposite side of the compression unit. The distal end of the bundle is bifurcated, and its two legs guide photons respectively to a PMT for the detection of VIS wavelengths (sensitive up to 850 nm, R5900U-01-L16, Hamamatsu, Japan) and to a PMT for NIR wavelengths (sensitive up to 1100 nm, H7422P-60, Hamamatsu, Japan). Variable neutral density circular filters, placed in front of each PMT, are used to optimize the illumination power for *in vivo* measurements and for the acquisition of the instrument response function, as changing the settings of the laser driver would affect the laser pulse duration and stability. Furthermore, a sector of the filter is covered with a black aluminum foil and operates as a shutter. A PC board for time-correlated single-photon counting (SPC134, Becker&Hickl, Germany) allows the acquisition of time-resolved transmittance curves. The illumination fiber and collecting bundle are scanned in tandem, and a feedback on the total number of counts per point, ruled by an adjustable threshold, restricts the scan to the breast area. To minimize dead times, continuous acquisition is performed and data are usually stored every millimeter of path, i.e., every 25 ms. A complete scan with a count rate of about 10^6 counts/s typically requires 5 min. The Plexiglas plates can be rotated by an angle up to 90 deg in both clockwise and counter-clockwise directions, so that images of both breasts can be recorded in the cranio-caudal (CC) as well as medio-lateral or oblique (OB) views. Further technical details can be found in Ref. 18.

Data analysis is performed with dedicated software. Images at four wavelengths are constructed by plotting the number of photons collected within a selected time window, as well as the reduced scattering coefficient. To avoid dependence of gated intensity images on the temporal position and width of single transmittance curves, instead of choosing a time window of fixed delay and width, we follow the procedure described in Ref. 19. Briefly, a reference position is chosen far from boundaries and eventual inhomogeneities. The time distribution of data acquired in that position is divided

Table 1 Types and number of lesions included in the study and classification for data analysis.

Lesion type	Number of cases	Classification for data analysis
Invasive ductal carcinoma	10	Cancer
Invasive lobular carcinoma	5	Cancer
Invasive lobular/ductal carcinoma	2	Cancer
Multicentric ductal carcinoma	1	Cancer
Mucinous carcinoma	1	Cancer
Ductal carcinoma *in situ*	1	Cancer
Paget's carcinoma	1	Cancer
Cyst	40	Cyst
Fibroadenoma	35	Fibroadenoma
Fibrolipoma	4	Other
Microcalcifications	4	Other
Parenchymal distorsion	4	Other
Fibroadenolipoma	2	Other
Lipoma	1	Other
Mastopathy	1	Other
Oedema post surgery	1	Other
Surgery scar	1	Other

into 10 time windows, each one collecting 1/10 of the total number of counts. The same time gates are then used in any other position of the scanned area to build gated intensity images. Specifically, the eighth gate, on the tail of the pulse, is routinely applied for breast imaging. The estimated absorption and reduced scattering coefficients (μ_a and μ_s') are average values along the line of sight, obtained from the best fit of the experimental data with the analytical solution of the diffusion equation, with extrapolated boundary condition, for a homogeneous slab.[20,21]

Data correction to account for edge effects, which are due to the variable thickness of the compressed breast in the boundary region, presently is not performed. However, this is not expected to limit significantly the diagnostic potential of the technique, as the acquisition of data in two different views allows us to image reliably the full breast volume.

Images are routinely displayed using the pink color scale (Matlab, The MathWorks Incorporated Natick, MA), which is a linear scale going from dark (low values) to white (high values).

The entire setup is a stand-alone instrument (50 cm W × 80 cm D × 140 cm H), called MAMMOT (MAMMograph for Optical Tomography), mounted on wheels and suitable for use in a clinical environment.

From November 2001 to October 2002, 101 patients were included in the clinical study. 21 malignant lesions and 93 benign lesions were analyzed. The different lesion types and their frequency are summarized in Table 1. As shown in the table, for data analysis, all malignancies were gathered. Among benign lesions, only cysts and fibroadenomas were considered separately. All other benign lesions or conditions were grouped in one category labeled "Other."

The measurement protocol was approved by the local ethics committee, and informed consent is obtained from all patients recruited for the clinical trial. Optical images are routinely acquired from both breasts in CC and OB (45-deg) views, to allow easy comparisons with the x-ray mammograms typically available (for clinical or screening assessment) in the same views for all patients. In several situations, especially with benign lesions, ultrasonography is also performed for better characterization, while, in the case of clinical or radiological evidence, or suspicion of malignancy, histopathological assessment is carried out. For two young patients (19 and 23 years old, respectively), x-ray mammography was not performed. However, histopathology was available in both cases.

3 Results and Discussion

3.1 *Visual Analysis of Images: Optical Features of Breast Structures and Lesions*

A retrospective study is being performed to allow us to define the optical appearance of different breast lesions and structures, with the final aim of determining effective diagnostic criteria. To this purpose we have analyzed comparatively x-ray and optical mammograms, always trying to recognize the same features in both types of images and, if possible, in both CC and OB views.

Late gated intensity images are used to represent the spatial variations of the absorption properties, instead of absorption plots. In particular, the light intensity in the eighth gate is routinely displayed. Such a gate is delayed enough to be essentially sensitive only to the absorption properties and not be significantly affected by edge effects. At the same time, the signal-to-noise ratio (SNR) is still adequate if the cw intensity image, obtained from the entire time distribution, has an acceptable signal level. The use of gated intensity images implies giving up any attempt to quantify, even approximately, the absorption properties of tissue. Such a choice was made because of the very limited spatial resolution and contrast of absorption images obtained using a homogeneous model to describe light transmission through the breast.[11] Moreover, the absorption plots are quite sensitive to changes in the scattering properties, due to some coupling of the two optical coefficients.[22]

The illumination wavelengths were selected to be sensitive to the four main constituents of tissue absorbing in the NIR: oxy- and deoxyhemoglobin, lipids, and water. A typical example of absorption spectrum measured on a 44-year-old volunteer is displayed in Fig. 1, together with the line shapes of the four constituents.[16] At short wavelengths, the absorption of tissue is dominated by the tail of deoxyhemoglobin, while oxyhemoglobin shows a very broad absorption band centered around 900 nm. As shown in Fig. 1, a sharp peak at 930 nm
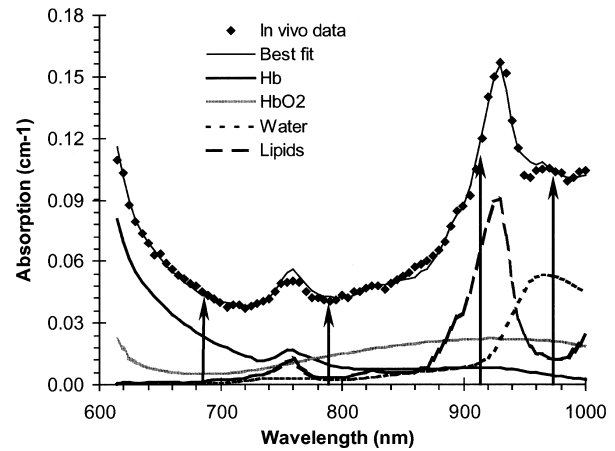

Fig. 1 Typical *in vivo* absorption spectrum of breast, measured from a healthy volunteer (44 year old) using time-resolved reflectance spectroscopy. The spectra of oxyhemoglobin (7.9 μM), deoxyhemoglobin (4.6 μM), lipids (71%), and water (12%), weighted by their concentration, are also shown. The four imaging wavelengths are marked.

characterizes the absorption of lipids, and water exhibits a maximum around 970 nm.

Based on the comparative analysis of x-ray and optical images, some typical optical signatures could be determined. First of all, the mammary gland, or its residual in elderly women, can usually be detected as a strongly attenuating structure (dark) in late gated intensity images at 975 nm. Taking into account the presence of the absorption maximum of water at 970 nm, this observation is in agreement with the predictably high water content of the mammary gland, as compared to the surrounding adipose breast tissue. Sometimes slightly lower scattering at 975 nm identifies the area of the mammary gland as well. Blood vessels, especially more superficial ones, are clearly detected as highly absorbing structures at 683 and 785 nm, where blood absorption is higher. At the two shorter wavelengths, a region of strong absorption is often detected in the nipple area, which can be attributed to high vascularization. For the same reason, close to the chest wall, especially in the OB view, the presence of the chest muscle causes strong light attenuation at 683 and 785 nm.

Similar to what was just reported, the optical features of some other structures and lesions could be anticipated based on their specific composition/nature, and then confirmed experimentally. As an example, lipomas, which are particularly lipid-rich regions, strongly attenuate light at 913 nm, i.e., close to the absorption peak of lipids at 930 nm. Figure 2 reports late gated intensity images (OB view) of a breast with a lipoma in the lower outer quadrant. For comparison, the corresponding x-ray mammogram is also displayed, showing the position of the mammary gland (opaque to x-rays) and of the lipoma (transparent). In the lower quadrants of the imaged breast, the lipoma appears lighter than the surrounding tissue (i.e., weakly attenuating) at all wavelengths except for 913 nm. At that wavelength, the lipoma does not differ significantly from neighboring areas. At 975 nm, the residual of the mammary gland can be identified as a dark, strongly absorbing area, located above the lipoma. The light area observed in the upper quadrants, close to the breast boundary, corresponds to an adipose region, essentially transparent to x-rays. This is

in agreement with the fact that weak absorption is observed in optical images at all wavelengths except for 913 nm. For what concerns the scattering plots, no significant spatial changes are noticed at the two shorter wavelengths, while the area of the mammary gland is characterized by low scattering at 975 nm. This is essentially the only scattering feature observed in healthy breasts, and is not always clearly detected. Low signal was collected at 913 nm, making the corresponding scattering plot rather noisy and preventing an accurate analysis of the scattering properties at that wavelength.

Liquid cysts are usually detected and identified quite easily thanks to their low scattering at any wavelengths, as shown in Fig. 3. In the scattering images at 975 nm, it is also possible to observe a dark region (low scattering), corresponding to the mammary gland, in agreement with what was observed before. In some cases, specific absorption features also identify cysts: typically high values at 683 and 975 nm, and low values at 785 and 913 nm. Concerning the wavelengths longer than 900 nm, the behavior can reasonably be explained by high water and low lipid concentrations, while the observations referring to shorter wavelengths are probably due to a high blood content, with low oxygen saturation. Actually, at 683 nm the absorption of deoxyhemoglobin is dominant, while at 785 nm it is comparable to (or even lower than) that of oxyhemoglobin. Strong absorption at the two shorter wavelengths, attributed to high blood content, is also observed close to the nipple. Similar behavior is quite common.

Two cysts in the external quadrants of the right breast are identified in the scattering images displayed in Fig. 4. One cyst, close to the breast edge, is partially obscured by the artificially low scattering values due to the edge effects. In this case, the absorption trend of the cysts at different wavelengths can hardly be recognized, and not independently, but only once the position of the lesion has been clearly defined from the scattering plots. Specifically, some reduction in absorption can be observed at 785 and 913 nm, corresponding to the cyst located deeper in the breast tissue.

Malignant lesions are often identified based on their marked absorption at the two shorter wavelengths, especially at 683 nm, as for the carcinoma in the left breast shown in Fig. 4. The contrast is usually lower at 785 nm than at 683 nm, but the image at the longer wavelength is often less structured, so even a lower contrast can, at least in some cases, be sufficient for tumor localization. The reason for the optical signature of most tumors is likely to be the neovasculature, which feeds the neoplastic mass accompanying its development.[23] Tumors, especially when a significant volume is involved, may also show lower scattering than surrounding healthy tissue. The onset and progression of disease severely affect tissue architecture, altering cell density and nuclear volume, degrading the extracellular matrix on invasion, and forming a complex network of new blood vessels. So, differences in scattering are conceivable, especially between well-differentiated normal tissue and poorly differentiated invasive tumors.

Fibroadenomas often absorb more than surrounding tissue at 683 and 975 nm, and less at 785 and 913 nm. Sometimes, the presence of a fibroadenoma seems to involve some reduction in scattering as well, which is more evident in the case of encapsulated fibroadenomas. However, these optical features are usually not all present at the same time, and the contrast is

Table 2 Definition of visibility scores.

Visibility score	Definition
5	Contrast dominates image
4	Contrast comparable to other inhomogeneities
3	Contrast inferior to other inhomogeneities, but still clearly identified
2	Weak contrast
1	Hardly perceivable inhomogeneity, only detected if position is known
0	Not visible

often quite low, hampering lesion detection. The measured absorption behavior is compatible with a high water and low lipid content, as compared to the surrounding adipose breast tissue. However, it should be taken into account that preliminary measurements of the optical properties of collagen between 600 and 1000 nm indicate high absorption both below 700 nm and above 950 nm, in agreement with what is observed in fibroadenomas. An example of images collected from a patient bearing a fibroadenoma is shown in Fig. 5. As compared to the surrounding tissue, the fibroadenoma is weakly absorbing at 785 and 913 nm, and comparably absorbing at 683 and 975 nm. Concerning the longest wavelength, it has to be noted that the fibroadenoma is surrounded by glandular tissue, as clearly seen in the x-ray mammogram. Thus, strong absorption at 975 nm is expected, which might mask the lesion absorption. A superficial blood vessel is clearly visible, especially at the two shorter wavelengths, because of the strong hemoglobin absorption. It can also be detected at the longest wavelength. As already observed in a previous case, here again the retroareolar region is characterized by strong absorption at 683 and 785 nm. Low scattering is detected in the region of the lesion, but also a second area with similar scattering properties is present. The latter one corresponds to no significant feature in the x-ray mammogram, suggesting a false positive detection. In some situations, false positive cases can be ruled out based either on the presence in just one view or in comparison with the controlateral breast. A very low scattering was observed in one case of fibroadenoma, which histology proved to be an encapsulated fibroadenoma. In that case, both the nature of the lesion and the capsule, acting as a waveguide for the injected light, might have contributed to the estimated low-scattering value.

3.2 Semiquantitative Data Analysis: Detection Rate as a Function of Lesion and Breast Features

3.2.1 Lesion detection

The visibility scores used to classify detected lesions, following the protocol of the clinical study, are reported in Table 2.[24] As typical examples, the visibility scores for the lesions shown in Figs. 2 through 5 are listed in Table 3, together with the image type they refer to. We regard a lesion as detected, if
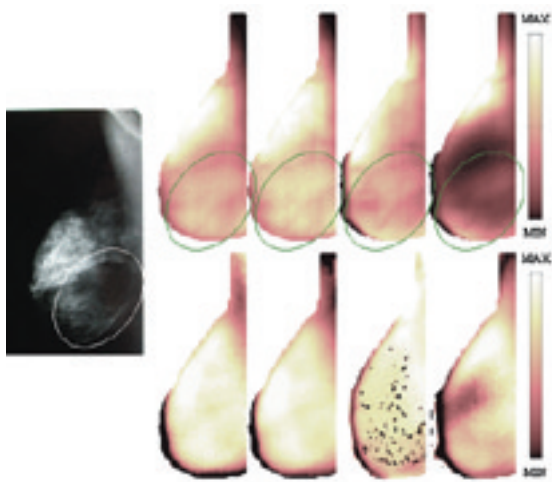
Fig. 2 OB view of the right breast of patient 11 with a lipoma (circled) in the lower outer quadrant. From left to right: x-ray mammogram, late gated intensity images (top), and scattering plots (bottom) at 683, 785, 913, and 975 nm. In optical images, dark indicates a low value: a low number of counts (i.e., strong absorption) in intensity images and low scattering in scattering plots. The color bar range (a.u.) for intensity images is 0.02 to 1.8 (683 nm), 0.06 to 1.4 (785 nm), 0.03 to 1.9 (913 nm), and 0.11 to 8.5 (975 nm); for scattering images (cm^{-1}), it is 15.6 to 27.0 (683 nm), 13.0 to 19.9 (785 nm), 5.8 to 8.5 (913 nm), and 2.8 to 8.6 (975 nm).

Fig. 4 CC views of both breasts of patient 43 [right breast with two cysts (20 mm max. diam each) in the upper outer quadrant (dashed arrows), left breast with a carcinoma (30 mm max. diam) in the upper outer quadrant (solid arrow)]. From left to right: x-ray mammogram, late gated intensity scattering images (top), and scattering (bottom) at 683, 785, and 913 nm. The images acquired at 975 nm are not reported because of the very low signal level. The color bar range (a.u.) for intensity images is 0.3 to 1.9 (683 nm), 0.6 to 1.5 (785 nm), and 0.5 to 3.5 (913 nm); for scattering images (cm^{-1}), it is 4.0 to 11.3 (683 nm), 4.0 to 9.3 (785 nm), and 4.0 to 10.8 (913 nm).
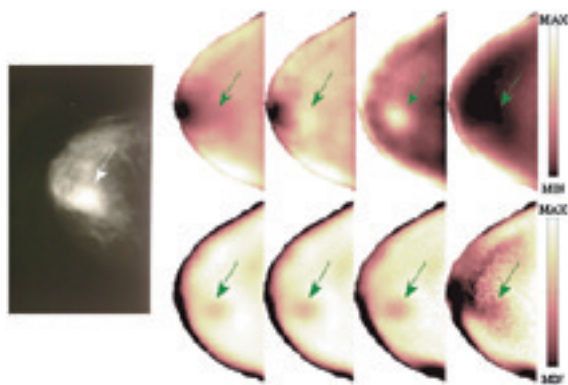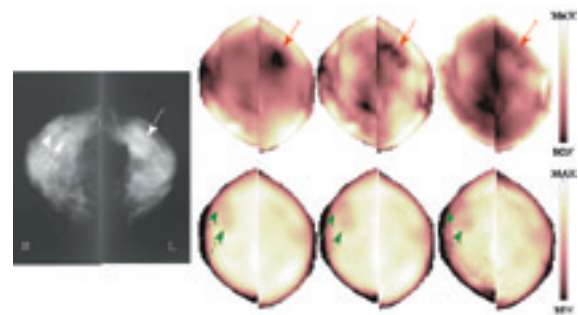

Fig. 3 CC view of the right breast of patient 57 with a cyst (35 mm max. diam) in the upper inner quadrant (arrow). From left to right: x-ray mammogram, late gated intensity images (top), and scattering images (bottom) at 683, 785, 913, and 975 nm. The color bar range (a.u.) for intensity images is 0.1 to 1.5 (683 nm), 0.2 to 1.2 (785 nm), 0.6 to 2.6 (913 nm), and 0.5 to 7.4 (975 nm); for scattering images (cm^{-1}), it is 4.2 to 13.6 (683 nm), 3.9 to 11.3 (785 nm), 4.3 to 12.5 (913 nm), and 3.4 to 11.9 (975 nm).
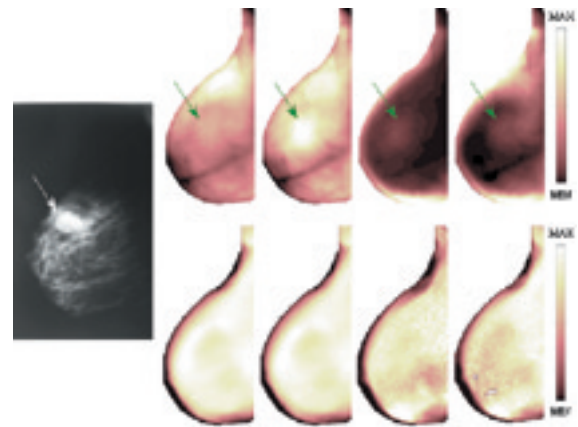

Fig. 5 OB view of the right breast of patient 71 with a fibroadenoma (25 mm max. diam) in the upper inner/outer quadrants (arrow). From left to right: x-ray mammogram, late gated intensity images (top), and scattering images (bottom) at 683, 785, 913, and 975 nm. The color bar range (a.u.) for intensity images is 0.2 to 1.7 (683 nm), 0.2 to 1.4 (785 nm), 0.4 to 9.7 (913 nm), and 0.2 to 4.2 (975 nm); for scattering images (cm^{-1}), it is 4.0 to 14.0 (683 nm), 4.0 to 11.0 (785 nm), 4.0 to 11.0 (913 nm), and 4.0 to 11.0 (975 nm).

Table 3 Visibility scores and image types they refer to for the lesions shown in Figs. 2–5.

Patient	Lesion type	Visibility score	Image type
11 (Fig. 2)	Lipoma	3	Intensity at 683 nm
57 (Fig. 3)	Cyst	5	Scattering at 683 to 913 nm
43 (Fig. 4)	Cancer	5	Intensity at 683 nm
43 (Fig. 4)	Cysts (both)	5	Scattering at 683 to 913 nm
71 (Fig. 5)	Fibroadenoma	4	Intensity at 785 nm

identified retrospectively in both views of the same image type (e.g., scattering plot at 975 nm), even though it does not correspond to the area with highest contrast in both images. Specifically, the visibility score has to be ≥2 in each view, leading to an overall score (sum of the values for the CC and OB views) ranging between 4 and 10 for the detection of the lesion. The visibility scores are attributed to the images (CC and OB views) that allow the easiest location of the lesion. As described previously, this occurs in different image types for different lesion types. As an example, cancers are generally best identified in intensity images at 683 nm. Table 4 reports the number of malignant and benign lesions that were correctly classified. As described earlier (Sec. 2), all malignancies were gathered, and among benign lesions only cysts and fibroadenomas were considered separately. Any other benign conditions (fibrolipoma, parenchyma distortion, mastopathy, etc.) were labeled "Other," because only a limited number of cases was available for each lesion type or condition, and no significant results would have been achieved considering them individually.

As shown in Table 4, overall 17 of 21 malignant lesions (i.e., 81%) were correctly identified. The detection rate for cysts seems lower (70%). However, it should be taken into account that in five cases of missed cyst detection, it turned out that the breast had not been correctly positioned for the measurements, and consequently the lesion was likely not included in the imaged area. If these cases are excluded, the rate of detection for cysts increases from 70 to 80%.

In the detection of fibroadenomas, we obtained our worst diagnostic results. Only 37% of these lesions could be detected in both CC and OB views. As described before, up to now we have not found optical features that could really be considered distinctive of fibroadenomas. This might be due to the fact that fibroadenomas can have different composition and structure, leading to different optical properties. It should also be taken into account that the most distinctive features seem to be weak absorption at 913 nm and strong absorption at 975 nm, the two wavelengths where we experienced more problems because of the low collected signal. So, the increase in the light power available at long wavelengths, which will be achieved as part of the technical upgrade presently underway, might also have a positive outcome on the detection rate of fibroadenomas. Moreover, if we could confirm that fibroadenomas have peculiar absorption properties at long wavelengths, this would be good for lesion characterization and identification, making fibroadenomas optically different from cysts and—even more important—from malignant lesions.

The detection of benign conditions labeled "Other" is very ineffective (33%), but it should be taken into account that, under this category, we list postsurgery oedemas, small microcalcifications, mastopathy, etc., which can differ very much from one another. Moreover, in some cases (e.g., mastopathy) they may not even be expected to differ optically from surrounding tissue. Consequently, to find effective criteria for their identification, a sufficient number of cases should be available for each type of condition/lesion, and they should be analyzed separately.

3.2.2 Visibility scores versus lesion size

The lesion size refers to the maximum lesion diameter, as estimated from the x-ray mammograms.

Table 4 Type, number, and average size of detected and missed lesions, and corresponding average thickness of the compressed breast (the last three columns report (average±standard deviation) values). In the average lesion size of a tumor (21±17), the size of two diffuse cancer lesions (one invasive lobular/ductal carcinoma and one multicentric ductal carcinoma) and a Paget's carcinoma in the nipple area could not be assessed reliably, so they were not included in the estimate of the average lesion size.

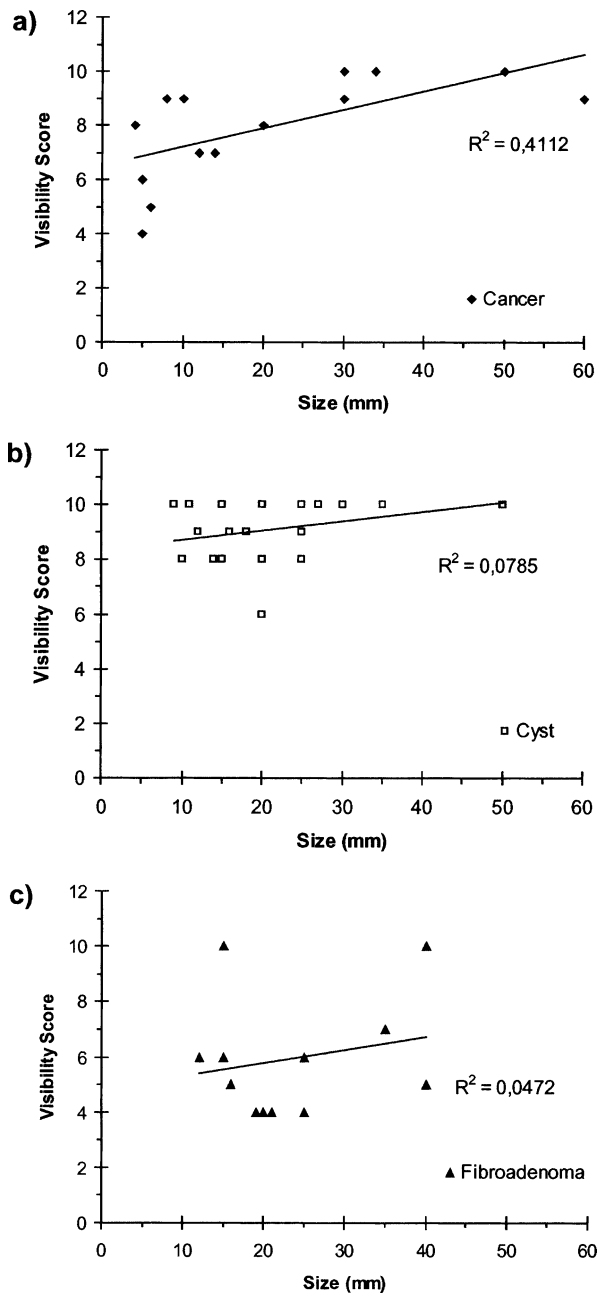| Lesion type	Detected	Number of cases	Average lesion size (mm)	Average breast thickness (mm)	Average size/thickness (%)
Tumor	Yes	17 (81%)	21±17	56±13	37±26
	No	4 (16%)	9±3	51±18	17±10
Cyst	Yes	28 (70%)	21±9	47±9	45±16
	No	12 (30%)	10±4	42±11	26±16
Fibroadenoma	Yes	13 (37%)	22±10	49±13	48±22
	No	22 (63%)	14 c 5	49±12	31±14
	Yes	6 (33%)	34±25	46±8	76±67
Other	No	12 (67%)	16±8	50±11	32±20

Fig. 6 Visibility scores versus lesion size for (a) cancers, (b) cysts, and (c) fibroadenomas.

As expected, it proved easier to detect lesions of bigger size, and this holds for any lesion type, even though data are quite scattered (Table 4). Also, the visibility scores for the detection of cancers show some increase with the lesion size [Fig. 6(a)], indicating a higher optical contrast. As already specified in Table 4, two cancer lesions (one invasive lobular/ductal carcinoma and one multicentric ductal carcinoma) were diffuse and one was a Paget's carcinoma in the nipple area. In all three cases, the size could not be reliably assessed from x-ray mammograms. So they are not shown in the figure. Other apparently missing cases in Fig. 6 and in the following figures are due to overlapping data. For cysts, the visibility scores are generally higher and seem not to depend signifi-

cantly on the lesion size [Fig. 6(b)]. This may be explained by taking into account that cysts are detected based on their low scattering, and the scattering maps of healthy breasts are usually quite flat, making the detection of a pathologic inhomogeneity easier. On the contrary, tumors are detected in intensity images, characterized by several structures (e.g., blood vessels, residual of the mammary gland, etc.), which may mask the presence of a lesion, hampering its detection. Data referring to fibroadenomas are quite scattered and not very numerous. So a clear trend cannot be derived [Fig. 6(c)]. On average, the visibility scores are quite low, confirming the present difficulty in the detection of this lesion type.

3.2.3 *Visibility scores versus breast thickness*

A reduction of the effectiveness in detecting a lesion when increasing the breast thickness would suggest that not enough light gets through thick breasts and reaches the detection apparatus. From data reported in Table 4, this seems not to be the case for any lesion type. The optical contrast of detected lesions, somehow quantified in the visibility scores, might indicate that the localization is easier in certain conditions. The scatter plots reported in Fig. 7 show the visibility scores as a function of breast thickness. A limited positive effect of thickness seems to exist in cancer detection, while no dependence is observed for benign lesions, either cysts or fibroadenomas. Overall, Table 4 and Fig. 7 hint that, once enough light is collected to build acceptable images, the possible low image quality due to the weak signal does not affect significantly the capacity to detect a lesion. However, it has to be noted that, for some patients with thick (59 ± 12 mm against 52 ± 10 mm) and/or dense breasts, at wavelengths longer than 900 nm, we could detect only a weak transmitted signal, which did not allow us to obtain reliable images. Only in one case, for a patient with a very dense breast, notwithstanding the limited thickness (30 mm), even at the two shorter wavelengths the signal collected was quite low, enough for acceptable intensity images, but not for reliable scattering plots. Figure 7 seems to suggest that malignant lesions can be localized with higher contrast in thick breasts. This might relate to the fact that thicker breasts are generally more adipose. From an optical point of view, tumors can be distinguished more easily from fatty tissue, absorbing over 900 nm, than from blood-rich glandular tissue, absorbing in the same wavelength range as malignant lesions due to the neovasculature. The situation is different for benign lesions that have different optical features, and seem not to be detected more favorably when surrounded by fatty tissue.

3.2.4 *Visibility scores versus (lesion size)/(breast thickness) ratio*

Due to the strong diffusion of light at optical wavelengths, the spatial resolution is limited to a few millimeters.[11,12] Small lesions are expected to be imaged as bigger than they actually are or not be detected at all, if characterized by a low optical contrast, as the effect of the optical inhomogeneity is washed out over a broad area. In practice, it proved difficult to detect tumors smaller than 10 mm, with an average size of 9 mm for missed lesions and 21 mm for detected ones (Table 4). A similar trend is observed also in the case of benign lesions. Actually, more than the absolute value of the lesion size, we
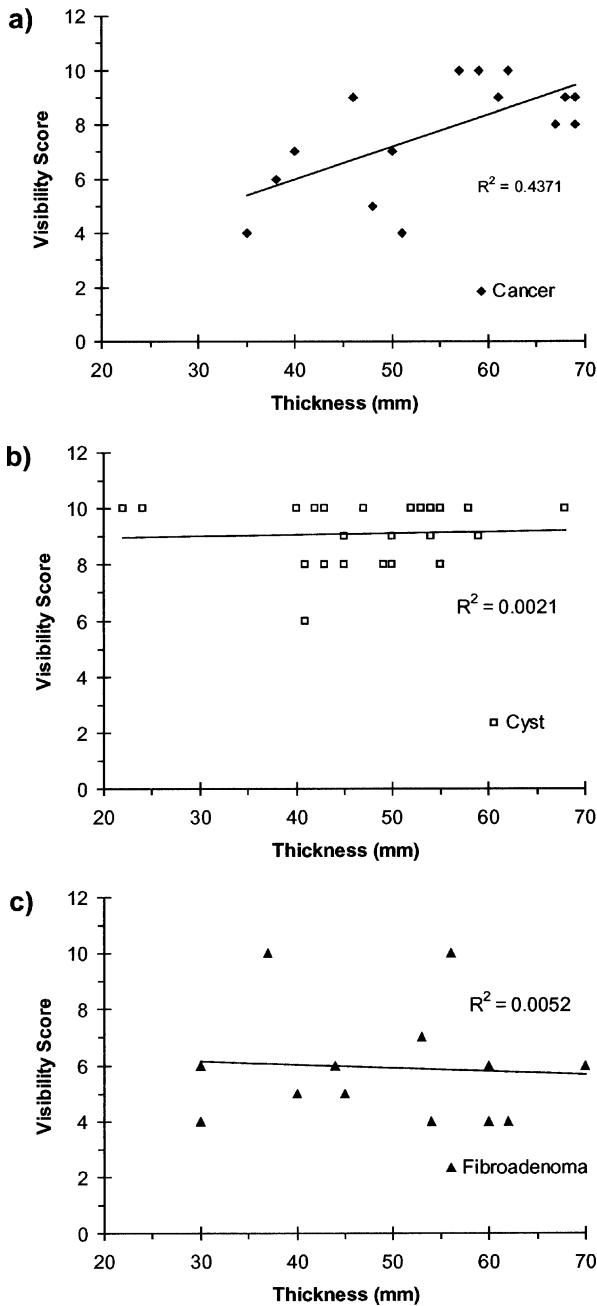
Fig. 7 Visibility scores versus breast thickness for (a) cancers, (b) cysts, and (c) fibroadenomas.

Fig. 8 Visibility scores versus ratio between lesion size and breast thickness for (a) cancers, (b) cysts, and (c) fibroadenomas.

should take into account its value relative to the thickness of the compressed breast. As a rough rule of thumb, we could say that when the light traverses the compressed breast, what really matters for the detection of a lesion is the percentage of the path the light takes within the lesion (Table 4). This holds both for intensity images and for scattering plots. In fact, in the latter case, to obtain an analytical solution to the problem, we interpret the experimental data with a simple theoretical model, which describes the breast tissue as a homogeneous slab. Thus, the estimated optical properties are average values over the light path. Hence, both lesion size and breast thickness contribute to determining the diagnostic potential of optical images. However, there are some exceptions to this
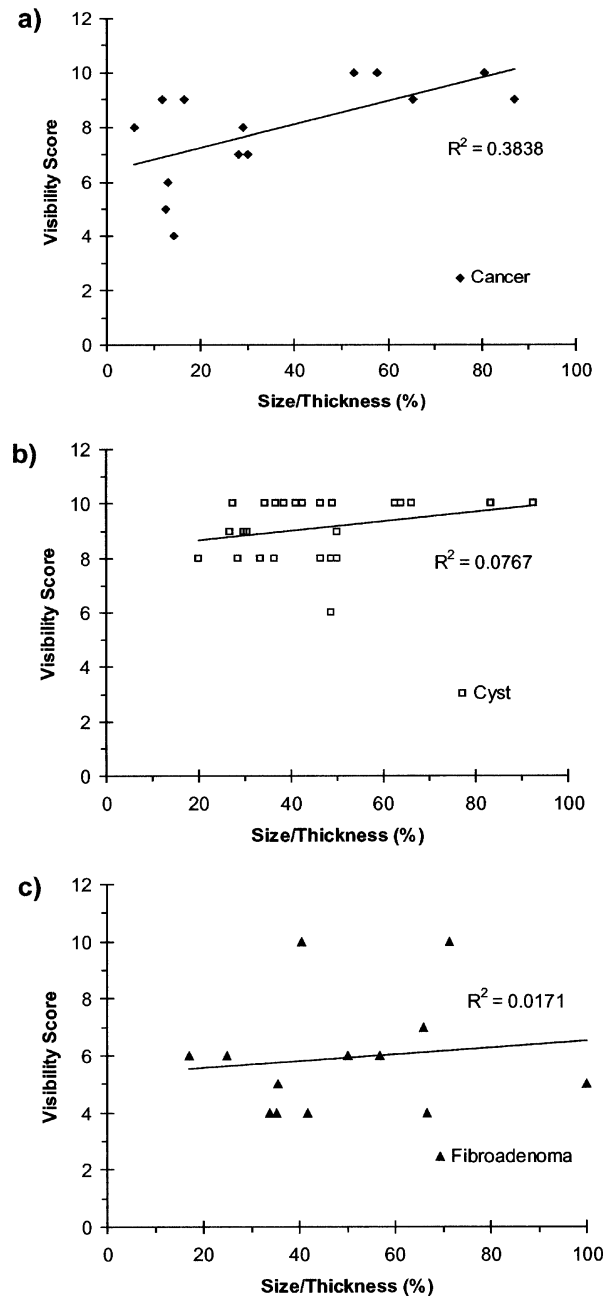
trend. Specifically, a 13-mm tumor could not be identified in a compressed breast of 45 to 48 mm thickness. To try to get some more insight, the dependence of the visibility scores on the ratio between lesion size and breast thickness was considered (Fig. 8). Again, only in the case of malignant lesions some trend seems to be present, with an increase in the detection contrast for higher values of the ratio. As noted earlier, it seems that tumors are usually detected based on the increased blood content, caused by neoangiogenesis associated with tumor development. When this phenomenon is not present, other specific features should be identified, possibly taking advantage also of the wavelengths longer than 900 nm. As mentioned before, in several cases, especially for young or

Table 5 Parenchymal pattern classification following Tabàr.[24]

Breast pattern	Definition
1	Comparable content of fibrous tissue, adipose tissue, linear densities (fibrous strands, blood vessels, milk ducts), and nodular densities (lobules)
2	Dominated by adipose tissue and linear densities
3	Similar to pattern 2, but with prominent retroareolar ducts
4	Dominated by prominent linear and nodular densities
5	Dominated by extensive fibrosis

thick breasts, data acquired at one or even both of the two longer wavelengths were characterized by low SNR. This reduced the informative content of the corresponding images or even made them unreliable. To get rid of this potential source of problems, a technical upgrade is now being performed to make sure that enough signal is collected at all wavelengths for any patient. The problem is not evident when the visibility scores for tumors against the average thickness of the breast are considered, possibly because the number of missed malignant lesions is very limited, and consequently the comparison of average breast thickness for detected and missed cancers cannot come to a definitive conclusion yet. Moreover, distinct breast types (adipose versus fibrous, etc.) are expected to attenuate light differently, but no clear predominance of a specific type was observed in the case of malignant lesions (even though the prior consideration on the limited number of available cases applies also to this observation).

3.2.5 Lesion detection versus parenchymal pattern

Five mammographic parenchymal patterns can be identified following Tabàr's classification (Table 5).[25] In particular, pattern 4 refers to a breast with prominent nodular densities (lobules) and linear densities (fibrous strands, blood vessels, or milk ducts), which make perception of lesions often difficult in radiographic images. On the other hand, in the case of optical images, cysts are detected at an even higher rate when located in a pattern 4 breast (78%, increasing to 88% if images suffering from bad breast positioning are excluded), as shown in Fig. 9(a). Due to the limited number of detected and missed lesions of other types (tumors or fibroadenomas) for each breast pattern [Fig. 9(b)], it is difficult to make reliable considerations in those cases. However, all tumors in type 2 and type 3 breasts were detected, in agreement with what was observed previously in easier detections of cancers in adipose breasts as compared to more fibrous ones.

Concerning images specifically discussed in the present work, patients 11 and 71 (Figs. 2 and 5, respectively) have breasts of type 4, while patients 57 and 43 (Figs. 3 and 4, respectively) have breasts with extensive fibrosis (type 5).
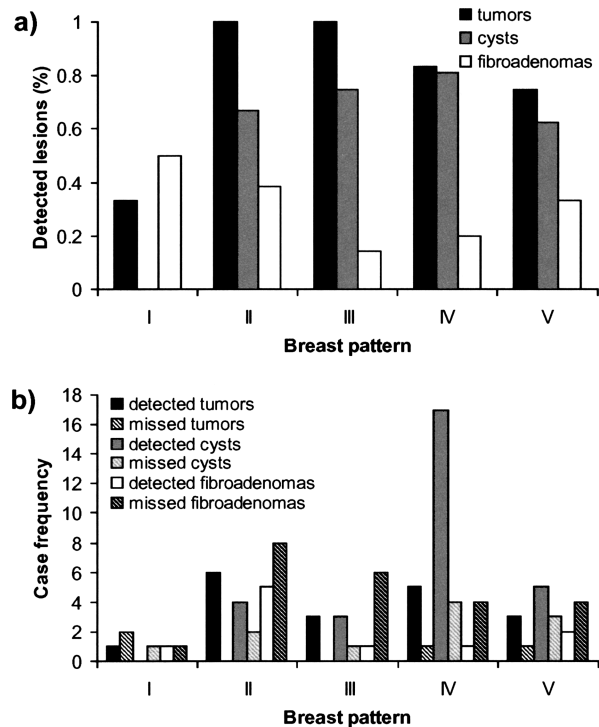
Fig. 9 Percentage of (a) detected lesions and (b) number of detected/missed lesions versus breast pattern for cancers, cysts, and fibroadenomas. Data refer to a subset of 95 lesions, due to missing x-ray mammograms (two patients) or unclear pattern attribution.

4 Conclusions

As the first part of a clinical study, we collected optical data from more than 100 patients with malignant and benign lesions. Images of gated intensity and effective scattering coefficient were obtained at 683, 785, 913, and 975 nm. Breast structures were identified from an optical point of view, and some distinctive optical features of the different breast lesions were also identified. 81% of malignant lesions could be detected in both CC and OB projections, with various contrast levels. Comparable results are achieved for cysts, if recognized cases of bad breast positioning are excluded, while at present, the situation is significantly worse for fibroadenomas.

The optical data acquired so far allowed us to highlight some elements that should be addressed to improve the diagnostic results achieved. This concerns both data acquisition and analysis. In particular, a technical upgrade of the instrument is on-going to improve the SNR, especially beyond 900 nm, where more problems were met. Moreover, a higher number of wavelengths will be tested, also trying to cover a broader spectral range. This will allow us to investigate whether better wavelengths exist both to detect and to differentiate different lesions.

At the same time, work is in progress on data analysis to exploit the spectral potential of optical imaging, as suggested in the Introduction in Sec. 1. Scattering maps presently used for lesion detection and shown in this work are obtained from a homogeneous model of photon propagation. If the estimated optical properties are to be used as input data for the assessment of tissue composition and physiological parameters of relevance for diagnostic purposes, the presence of optical het-

erogeneities should be accounted for. In this line, we have recently developed a nonlinear perturbation model.[26] Preliminary application to *in vivo* data[27] showed promise, and now we plan to extend it to a wide number of cases to obtain statistically significant data on optical properties and physiologic parameters of breast tissue and lesions.

Acknowledgment

References

1. A. Alveryd, L. Andersson, K. Aspegren, G. Balldin, N. Bjurstam, G. Edstrom, G. Fagerberg, U. Glas, O. Jarlman, and S. A. Larsson, "Lightscanning versus mammography for the detection of breast cancer in screening and clinical practice. A Swedish multicenter study," *Cancer* **65**, 1671–1677 (1990).
2. G. E. Geslien, J. R. Fisher, and C. De Laney, "Transillumination in breast cancer detection: screening failures and potential," *AJR, Am. J. Roentgenol.* **144**, 619–622 (1985).
3. J. J. Gisvold, L. R. Brown, R. G. Swee, D. J. Raygor, N. Dickerson, and M. K. Ranfranz, "Comparison of mammography and transillumination light scanning in the detection of breast lesions," *AJR, Am. J. Roentgenol.* **147**, 191–194 (1986).
4. H. Dehghani, B. W. Pogue, S. P. Poplack, and K. D. Paulsen, "Multiwavelength three-dimensional near-infrared tomography of the breast: initial simulation, phantom, and clinical results," *Appl. Opt.* **42**, 135–145 (2003).
5. H. Jiang, Y. Xu, N. Iftimia, J. Eggert, K. Klove, L. Baron, and L. Fajardo, "Three-dimensional optical tomographic imaging of breast in a human subject," *IEEE Trans. Med. Imaging* **20**, 1334–1340 (2001).
6. V. Ntziachristos, A. G. Yodh, M. Schnall, and B. Chance, "Concurrent MRI and diffuse optical tomography of breast after indocyanine green enhancement," *Proc. Natl. Acad. Sci. U.S.A.* **97**, 2767–72 (2000).
7. S. B. Colak, M. B. van der Mark, G. W. Hooft, J. H. Hoogenraad, E. S. van der Linden, and F. A. Kuijpers, "Clinical optical tomography and NIR spectroscopy for breast cancer detection," *IEEE J. Sel. Top. Quantum Electron.* **5**, 1143–1158 (1999).
8. K. T. Moesta, S. Fantini, H. Jess, S. Totkas, M. A. Franceschini, M. Kaschke, and P. M. Schlag, "Contrast features of breast cancer in frequency-domain laser scanning mammography," *J. Biomed. Opt.* **3**, 129–136 (1998).
9. L. Götz, S. H. Heywang-Köbrunner, O. Schütz, and H. Siebold, "Optical mammography on preoperative patients (Optische Mammographie an pra¨operativen Patientinnen)," *Aktuelle Radiol.* **8**, 31–33 (1998).
10. D. Grosenick, K. T. Moesta, H. Wabnitz, J. Mucke, C. Stroszczynski, R. Macdonald, P. M. Schlag, and H. Rinneberg, "Time-domain optical mammography: initial clinical results on detection and characterization of breast tumors," *Appl. Opt.* **42**, 3170–3186 (2003).
11. A. H. Gandjbakhche, R. Nossal, and R. F. Bonner, "Resolution limits for optical transillumination of abnormalities deeply embedded in tissues," *Med. Phys.* **21**, 185–191 (1994).
12. S. Behin-Ain, T. van Doorn, and J. R. Patterson, "Spatial resolution in fast time-resolved transillumination imaging: an indeterministic Monte Carlo approach," *Phys. Med. Biol.* **21**, 2935–2945 (2002).
13. A. E. Cerussi, D. Jakubowski, N. Shah, F. Bevilacqua, R. lanning, A. J. Berger, D. Hsiang, J. Butler, R. F. Holecombe, and B. J. Tromberg, "Spectroscopy enhances the information content of optical mammography," *J. Biomed. Opt.* **7**, 60–71 (2002).
14. N. Shah, A. Cerussi, C. Eker, J. Espinoza, J. Butler, J. Fishkin, R. Hornung, and B. Tromberg, "Noninvasive functional optical spectroscopy of human breast tissue," *Proc. Natl. Acad. Sci. U.S.A.* **98**, 4420–4425 (2001).
15. R. Cubeddu, C. D'Andrea, A. Pifferi, P. Taroni, A. Torricelli, and G. Valentini, "Effects of the menstrual cycle on the visible and near infrared optical properties of the human breast," *Photochem. Photobiol.* **72**, 383–391 (2000).
16. R. Cubeddu, A. Pifferi, P. Taroni, A. Torricelli, and G. Valentini, "Non-invasive absorption and scattering spectroscopy of bulk diffusive media: An application to the optical characterization of human breast," *Appl. Phys. Lett.* **74**, 874–876 (1999).
17. B. J. Tromberg, N. Shah, R. Lanning, A. Cerussi, J. Espinosa, T. Pham, L. Svaasand, and J. Butler, "Non-invasive in vivo characterization of breast tumors using photon migration spectroscopy," *Neoplasia* **2**, 26–40 (2000).
18. A. Pifferi, P. Taroni, A. Torricelli, F. Messina, R. Cubeddu, and G. Danesini, "Four-wavelength time-resolved optical mammography in the 680 to 980 nm range," *Opt. Lett.* **28**, 1138–1140 (2003).
19. D. Grosenick, H. Wabnitz, H. Rinneberg, K. T. Moesta, and P. Schlag, "Development of a time-domain optical mammograph and first in vivo applications," *Appl. Opt.* **38**, 2927–2943 (1999).
20. M. S. Patterson, B. Chance, and B. C. Wilson, "Time-resolved reflectance and transmittance for the noninvasive measurement of tissue optical properties," *Appl. Opt.* **28**, 2331–2336 (1989).
21. R. C. Haskell, L. O. Svasaand, T. T. Tsay, T. C. Feng, M. S. McAdams, and B. J. Tromberg, "Boundary conditions for the diffusion equation in radiative transfer," *J. Opt. Soc. Am. A* **11**, 2727–2741 (1994).
22. R. Cubeddu, A. Pifferi, P. Taroni, A. Torricelli, and G. Valentini, "Imaging of optical inhomogeneities in highly diffusive media: discrimination between scattering and absorption contributions," *Appl. Phys. Lett.* **69**, 4162–4164 (1996).
23. G. Bergers and L. Bejamin, "Tumorigenesis and the angiogenic switch," *Nature Rev.* **3**, 401–410 (2003).
24. K. T. Moesta, Clinical trial design group, within the OPTIMAMM Project, Robert Rössle Klinik, Charité, Berlin (2001).
25. I. T. Gram, E. Funkhouser, and L. Tabar, "The Tabàr classification of mammographic parenchymal patterns," *Eur. J. Radiol.* **24**, 131–136 (1997).
26. L. Spinelli, A. Torricelli, A. Pifferi, P. Taroni, and R. Cubeddu, "Experimental test of a perturbation model for time-resolved imaging in diffusive media," *Appl. Opt.* **42**, 3145–3153 (2003).
27. A. Torricelli, L. Spinelli, A. Pifferi, P. Taroni, and R. Cubeddu, "Use of a nonlinear perturbation approach for in vivo breast lesion characterization by multiwavelength time-resolved optical mammography," *Opt. Express* **11**, 853–867 (2003).